applied optics

Woofer–tweeter deformable mirror driven by combined actuators with a piezoelectric unimorph and stack for astronomical application

Junjie Chen,[1] Jianqiang Ma,[1,2] Heng Zuo,[3] Xiangyan Yuan,[3] Baoqing Li,[1,*] and Jiaru Chu[1]

[1]Department of Precision Machinery and Precision Instrumentation, University of Science and Technology of China, Hefei 230027, China
[2]Faculty of Mechanical Engineering and Mechanics, Ningbo University, Ningbo 315211, China
[3]National Astronomical Observatories, Nanjing Institute of Astronomical Optics & Technology, Chinese Academy of Sciences, Nanjing 210042, China
*Corresponding author: bqli@ustc.edu.cn

Received 8 January 2019; revised 24 February 2019; accepted 25 February 2019; posted 26 February 2019 (Doc. ID 357056); published 19 March 2019

A woofer–tweeter deformable mirror (DM) driven by combined actuators with a piezoelectric unimorph and stack for astronomical applications is proposed. The piezoelectric unimorph "tweeter" part, made of a 200-μm-thick lead zirconate titanate film and 200-μm-thick silicon, has 234 separate elements for high-order correction. It is magnetically jointed with a seven-element "woofer" piezo-stack array, which is for low-order correction. The combined DM was fabricated and experimentally evaluated, showing a high resonant frequency near 1 kHz. The piezo-stack array together with the unimorph actuators enable the DM to produce wavefronts with RMS residue errors less than 20 nm. Experimental results indicate that the woofer–tweeter DM has the capability to compensate for the first 35 terms of Zernike aberrations with normalized RMS wavefront errors less than 20%. The woofer–tweeter DM has higher bandwidth than a conventional unimorph DM as well as simple structure, low cost, and good scalability, offering a potential alternative for large-aperture astronomical applications.

https://doi.org/10.1364/AO.58.002358

1. INTRODUCTION

Development of the active and adaptive optics (AO) has allowed the construction of telescopes with primary mirrors more than 10 m in diameter, especially the European Extremely Large Telescope (E-ELT) [1] and the North American Thirty Meter Telescope (TMT) [2] under construction, which have primary mirrors on the order of 30–50 m. The degradation of astronomical images caused by atmospheric turbulence will be much more severe in the next generation of terrestrial telescopes. The increasing diameter of primary mirrors will result in the increase of the aberrations introduced by atmospheric turbulence. To compensate for the increasing aberrations, large-aperture AO with high correction precision and high bandwidth are required in astronomy. Deformable mirrors (DM), as typical devices of AO, are widely used in astronomical applications [3–5]. The state-of-the-art DMs and developing DMs for next-generation telescopes are mainly voice-coil DM [6,7] and piezo-stack DM [8,9]. Under the support of a dense piezo-stack array or voice-coil array, the piston-actuated mirrors have both large aperture and very high bandwidth. However, the disadvantages are the very high fabrication difficulty and high cost.

Bimorph/unimorph DMs have the advantages of having a large stroke, being lightweight, and being low cost. Bimorph DMs have been successfully used in telescopes [10,11]. It is estimated that the stroke/weight ratios of other DMs (~0.01 μm/g) are 1 order of magnitude lower than those of unimorph\bimorph DMs (~0.1 μm/g). Conventional bimorph\unimorph DMs are fixed or simply supported on the margin of the shell structure. Therefore, the inherent frequency of the conventional bimorph/unimorph DM is decreased with the increase of aperture diameter. As a result, the response speed of the large-aperture bimorph/unimorph DMs cannot meet the requirement of large-aperture astronomical applications. For example, the bimorph DM used in the multi-application curvature adaptive optics system (MACAO) has a low resonant frequency of 530 Hz [12]. The authors pointed out that the resonance frequency is the major driver in reducing the diameter of the mirror from the normal rule of thumb. A unimorph DM with an aperture of 50 mm was presented in our previous work [13,14]. The modified low-cost positive-voltage-driven unimorph DM showed good correction capabilities for both low-order and high-order Zernike aberrations, which is

attractive for astronomical applications. Nevertheless, the first resonance frequency of the presented DM is only 690 Hz. Low first resonance frequency limits the bandwidth of the unimorph DM as well as its applications in astronomy.

In addition to high bandwidth, the DM also requires a large stroke and high spatial frequency for atmospheric applications. To compensate for the large aberrations with high precision, woofer–tweeter control architectures have been studied for application on AO systems [15,16]. In these AO systems, two separate DMs are used: one for the low-order and large-amplitude parts of the wavefront and the other for the high-order and smaller-amplitude components. However, employing two DMs in series requires a longer light path, which will degrade the light intensity and take up more space in astronomical applications. It would be idea if there were a single DM with a large stroke and high spatial frequency that could realize the woofer–tweeter control architectures. Moreover, housing the high-order and low-order correctors inside a single element allows savings in the optical design and in the overall system complexity for complex astronomical systems.

To develop a DM with a large aperture, large stroke, high spatial frequency, and high bandwidth for astronomical applications, a woofer–tweeter DM driven by combined actuators with a piezoelectric unimorph and stack is proposed. Instead of fixed or simple support on the margin, a sparse actuator array is jointed with the unimorph part. The woofer–tweeter DM has the advantages of both the unimorph DM and piston-actuated DM. The sparse actuator array increases the structural stiffness while maintaining the advantages of the unimorph DM, including high resolution, large stroke, and low cost, and light weight.

2. WOOFER–TWEETER DEFORMABLE MIRROR

A. Structural Design

The layout of the woofer–tweeter DM is illustrated in Fig. 1. The DM is driven by both the unimorph part and the actuator array part. The unimorph part has a high spatial resolution but low temporal frequency, while the actuator array part has high temporal frequency but low spatial resolution. The unimorph part of the woofer–tweeter DM has a lower bandwidth than the actuator array part. Nevertheless, when comparing with unimorph or bimorph DMs, the unimorph part of the woofer–tweeter DM has a much higher bandwidth. Due to the constraint of the bottom actuator array, the inherent frequency of the top unimorph part depends on the arrangement of the actuator array rather than depending on its diameter. The problem of achieving both high spatial resolution and high temporal frequency is solved using the woofer–tweeter structure. Moreover, the woofer–tweeter structure provides the DM a scalable diameter while maintaining high bandwidth.

The unimorph part mainly comprises a lead zirconate titanate (PZT) layer and a silicon layer. On the top of the silicon layer, a reflector layer can be coated for high reflectivity according to application requirements. The surfaces of the PZT layer are covered by metal electrodes. The metal electrode on the backside is patterned to produce 234 hexagon electrodes. When voltages are applied on the electrodes, the PZT layer tries to expand/contract in the plane. Nevertheless, the expansion/constriction is limited by the silicon layer. As a result, out-of-plane deformations are generated under the in-plane actuation of the piezoelectric unimorph. To improve the initial profile quality of the mirror, a kind of thread adjustment mechanism with resolution of 1 μm is proposed in this work. The thread mechanism can adjust along the direction perpendicular to the mirror before testing and applications. Two parts of the woofer–tweeter DM is connected using magnet pillars. To avoid the stresses introduced by the connecting contact degrading the mirror profile quality, a spherical cap ceramic is sandwiched between the magnet pillars. The piezoelectric stacks mounted under the connection magnets provide out-of-plane forces to deform the mirror.

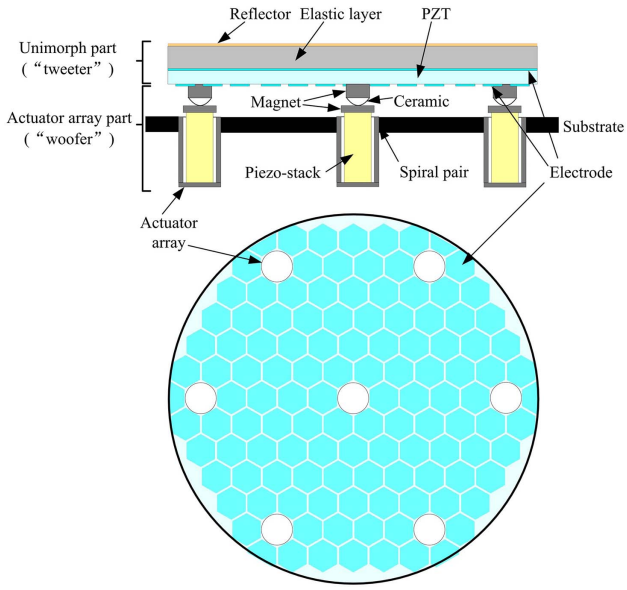

Fig. 1. Layout of the woofer–tweeter DM.

B. Analysis and Optimization

The bandwidth of the woofer–tweeter DM is determined by its inherent frequency, which is related to the arrangement of the actuator array part. The actuator array is arranged evenly and topologically, i.e., every three actuators form an equilateral triangle, in the analysis of the influence of the piezo-stack array. The relationship between the inherent frequency and the actuator number of the array with the DM diameter in 100 mm was simulated using the finite element method (FEM). The simulation results shown in Fig. 2 shows that the resonant frequency is proportional to the actuator number of the actuator array part, while the deformation of the single unimorph actuator is the opposite. In other words, the woofer–tweeter can increase of the resonant frequency at the price of the decrease of deformation. In this way, the woofer–tweeter DM can be designed to have a much higher bandwidth than a unimorph or bimorph DM. Nevertheless, the deformation is also a very important aspect of performance of the DM. By choosing a suitable actuator number and optimizing the actuator arrangement, we can design a woofer–tweeter DM that has high bandwidth and enough deformation for astronomical applications.

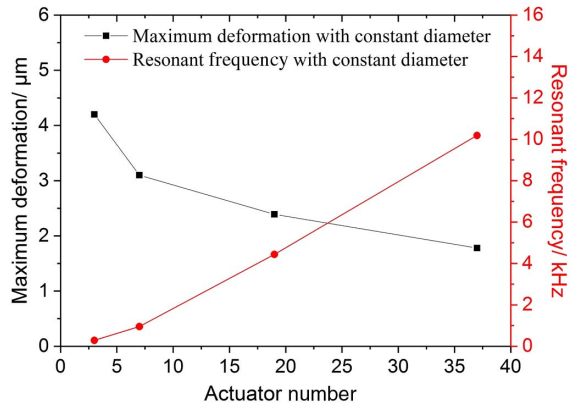

Fig. 2. Simulative maximum deformation of unimorph actuators and the resonant frequency of the woofer–tweeter DM in function of actuator number.

The influence of the PZT layer and the Si layer were also simulated. Figure 3 shows that the resonant frequency of the DM increases with the thickness of the PZT layer and the Si layer. To increase the resonant frequency of the DM, larger thicknesses of the PZT layer and the Si layer are demanded. However, larger thicknesses of the PZT layer and the Si layer will result in smaller deformation. The structure parameters of the unimorph part should be decided considering both the requirements of bandwidth and deformation. For a woofer–tweeter DM with diameter of 100 mm, the optimized thickness of the PZT layer and the Si layer are 200 μm and 400 μm, respectively. From the simulation mentioned above, the inherent frequency of the woofer–tweeter DM is about 796.3 Hz. The 234 hexagonal unimorph actuators with a diameter of 6 mm has seven piezo-stack actuators are arranged hexagonally.

3. FABRICATION

As shown in Fig. 4, a prototype of the woofer–tweeter DM was composed of two parts. Figure 4(a) shows the flow chart of the fabrication processes. The fabrication process of the unimorph part was quite similar to the one proposed in our previous work [14,17]. A 200-μm-thick PZT film and a 400-μm-thick silicon elastic layer were bonded together. The metal electrode on the backside of the PZT layer was patterned to produce 234 hexagon electrodes, which were arranged hexagonally. Then the connection pillars were bonded onto the unimorph part. Every connection pillar was arranged to replace a hexagonal actuator without changing the hexagonal distribution of the actuators. In the electrode pattern processes, alignment marks around the place where connection pillars were also formed. The alignment marks were aligned with the connection pillars during the bonding processes to ensure the assembly accuracy. To optimize the mirror quality by controlling the bond stress, the bonding processes of the unimorph part were performed at room temperature. The connection pillars consist of a magnet pillar and a spherical cap ceramic bonding together. The patterned electrodes were electrically connected with a flexible printed circuit after the fabrication process of the unimorph part, as shown in Figs. 4(b) and 4(c).

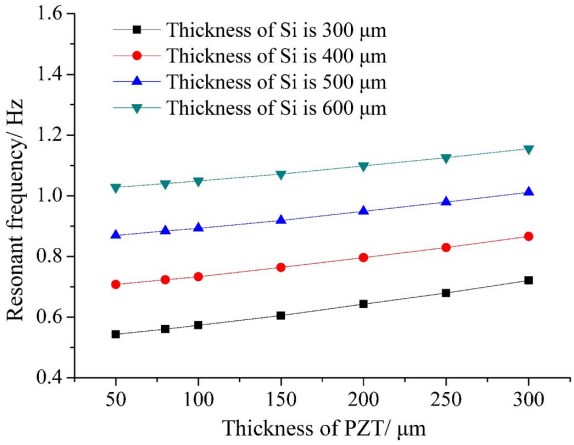

Fig. 3. Simulative resonant frequency of the woofer–tweeter DM in function of PZT thickness at different Si thicknesses.

For the actuator array part, seven high precision threaded holes with a screw pitch of 0.25 mm were fabricated, as shown in Fig. 4(d). Seven housing structures with external thread are matched with the base by threads. The housing structure can move along the vertical direction with mobile precision of 1 μm. After the piezo-stack and the housing structure were assembled together, a magnetic disk was bonded onto the top of the piezo-stack. During the mounting process, the magnet pillars on the top of the piezo-stacks are accurately positioned to align the magnet pillars on the unimorph part. Figure 4(e) shows the fabricated DM mounted on a measurement system.

4. CHARACTERIZATION

A. Actuator Performance

We have developed an optical train for DM testing, called an AO test system, which is described in the previous paper [14]. The wavefront of the beam reflected from the DM is measured using a Shack–Hartmann wavefront sensor (Thorlabs WFS 150-5C). The AO test system is a typical AO system, which can measure the influence function (IF) and perform adaptive closed-loop correction using the DM.

To evaluate the deformation capabilities of the woofer–tweeter DM, the wavefront deformation of the single actuator, also known as influence function, was measured in the AO test system. It is noted that the aperture of the DM in the measurement and the following experiments is about 70 mm in diameter due to the limitation of the AO test system. The measured deformations of four typical actuators along the radial direction and its measurement deformation in the cross section are shown in Fig. 5(a) and 5(b), respectively. The peak values of measurement deformations are around 0.8–2.7 μm when actuated at 50 V. The deformations also show a large valley value, called the reverse deformation phenomenon in this paper, especially for the actuator near the DM center. Due to the constraints of the piezo-stacks, the actuators of the woofer–tweeter DM generate positive and negative deformations. The reverse deformation phenomenon can also be seen in the simulation deformations shown in Fig. 5(c). The peak value difference and the valley value difference of the measurement and

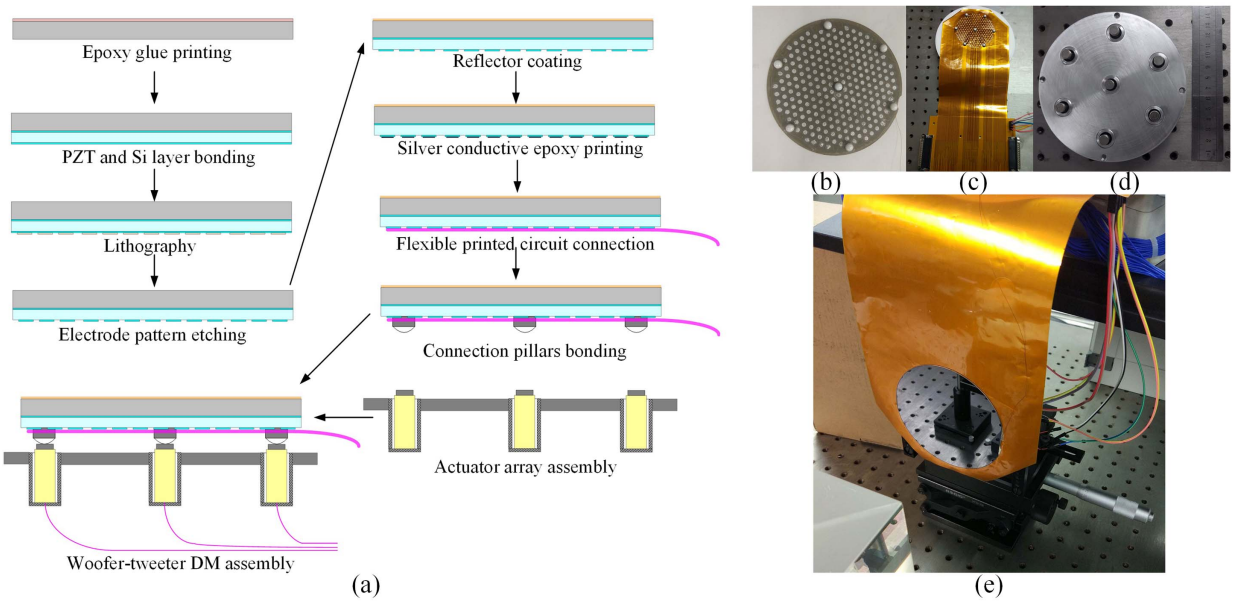

Fig. 4. Fabrication process of the woofer–tweeter DM. (a) Flow chart of the fabrication processes, (b) connection point array of silver colloid fabricated by using silk-screen printing, (c) electrical connections using a flexible printed circuit, (d) assembled piezo-stack array, and (e) fabricated DM mounted on AO test system.

simulative results are less than 0.46 μm and 0.11 μm, respectively. The reason for the acceptable differences is the simplicity of the structure in the simulation. The inner actuator near the center and the outer actuator near the edge have smaller deformation but larger reverse deformation than the actuators between them. The reason is that the inner actuator and the outer actuator are closer to the support pillars. The support structure increases the stiffness of the mirror, which helps to increase the inherent frequency. However, the increase of stiffness has the disadvantage of limiting the deformation of the actuators around the support pillars. From the comparison of Figs. 5(b) and 5(c), the measurement results show smaller deformation and slighter reverse deformation than the simulative results. The reason is that the contact of two parts and the magnet connection were simplified in the simulation. The deformations of the center actuator and one of the outer actuator of the actuator array are shown in Fig. 5(d). When actuated at 10 V, the peak-to-valley (PV) values are 3.27 μm and 2.59 μm, respectively.

B. Bandwidth

The experimental resonant frequency was measured using an optical heterodyne laser vibrometer (Neoark MLD-221D), when a swept-frequency voltage of 0.5 V was applied on the typical actuators. The amplitude responses of the woofer–tweeter DM are shown in Fig. 6(b). To ensure measurement accuracy, eight actuators shown in Fig. 6(a) are measured in the experiment. The response curve shows that the first resonant frequency is about 950 Hz. To test the effect of the support pillar, we artificially removed the center support actuator as a control group. The response curves of the incomplete woofer–tweeter DM with the center support pillar removed are tested and shown in Fig. 6(c). With only six support pillars, the first resonant frequency of the incomplete DM decreases from 950 Hz to about 400 Hz, compared with that of woofer–tweeter DM in normal operating conditions. The experiment results prove that increasing the density of support pillar distribution has the advantage of increasing the inherent frequency of the woofer–tweeter DM.

As mentioned in the introduction section, the first resonant frequency of the conventional unimorph DM in our previous work is about 690 Hz. The conventional unimorph DM and the woofer–tweeter DM have the same mirror diameter of 100 mm and similar support diameters of 90 mm and 88 mm, respectively. Compared with the conventional unimorph DM, the first resonant frequency of the woofer–tweeter DM has an improvement of 32.9%. Moreover, when the diameter of the DM is further scaled, the first resonant frequency of the woofer–tweeter DM with the same arrangement will not change significantly, while the first resonant frequency of the conventional unimorph DM will degrade sharply. The key technologies of developing woofer–tweeter DMs of larger aperture are under research. For example, we are trying to fabricate much larger PZT films with large thicknesses by assembling PZT segments together, just like the assembly of the primary mirror of the Keck telescope of 10 m with 36 individual segments [18].

C. Correction Capabilities

The correction capabilities of DM can be evaluated intuitively by a flattening experiment. In this paper, the flattening experiment is performed in the AO test system mentioned above. The slight aberration introduced by the AO test system was corrected together with the aberration introduced by the initial DM surface. Figure 7(a) shows the evolution of the residual root mean square (RMS) wavefront error and the wavefront aberrations before and after flattening. The aberrations are compensated to less than 50 nm wavefront RMS within 10

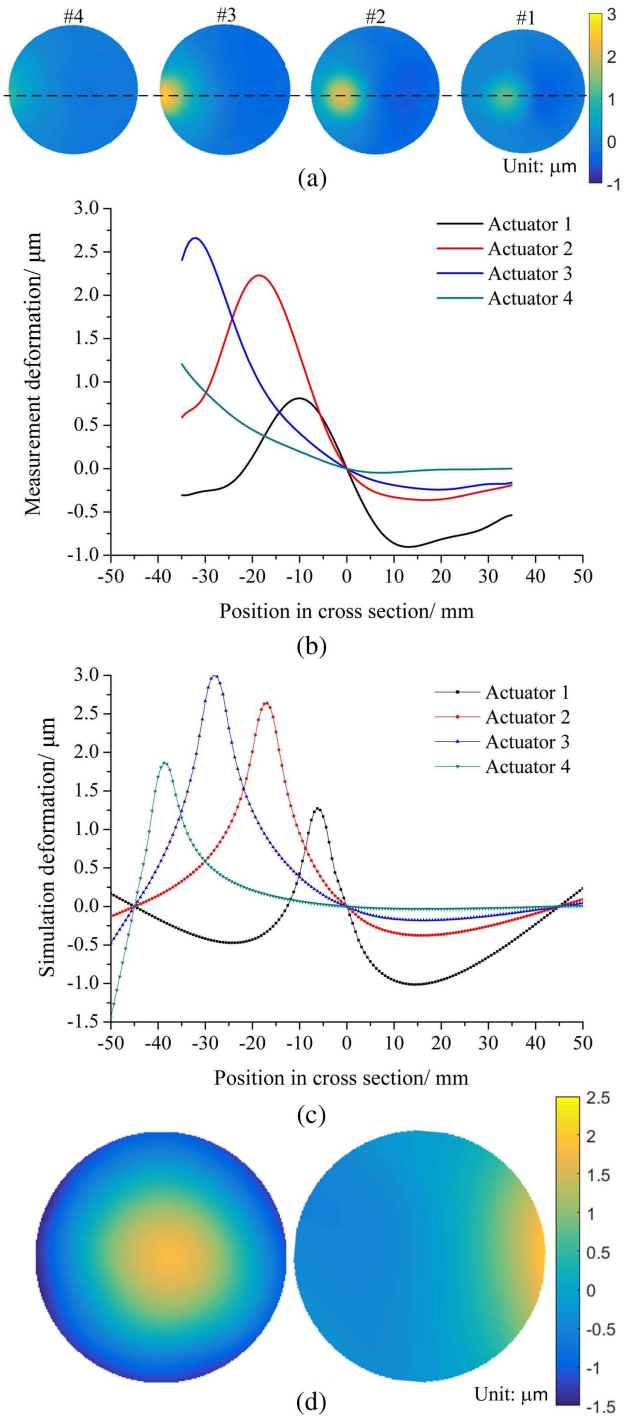

Fig. 5. Influence function of the typical inner actuators and actuator array. (a) Measured wavefronts at 50 V, (b) measured deformations in cross section, (c) simulated deformations in cross section, and (d) deformations of typical actuators of the actuator array.

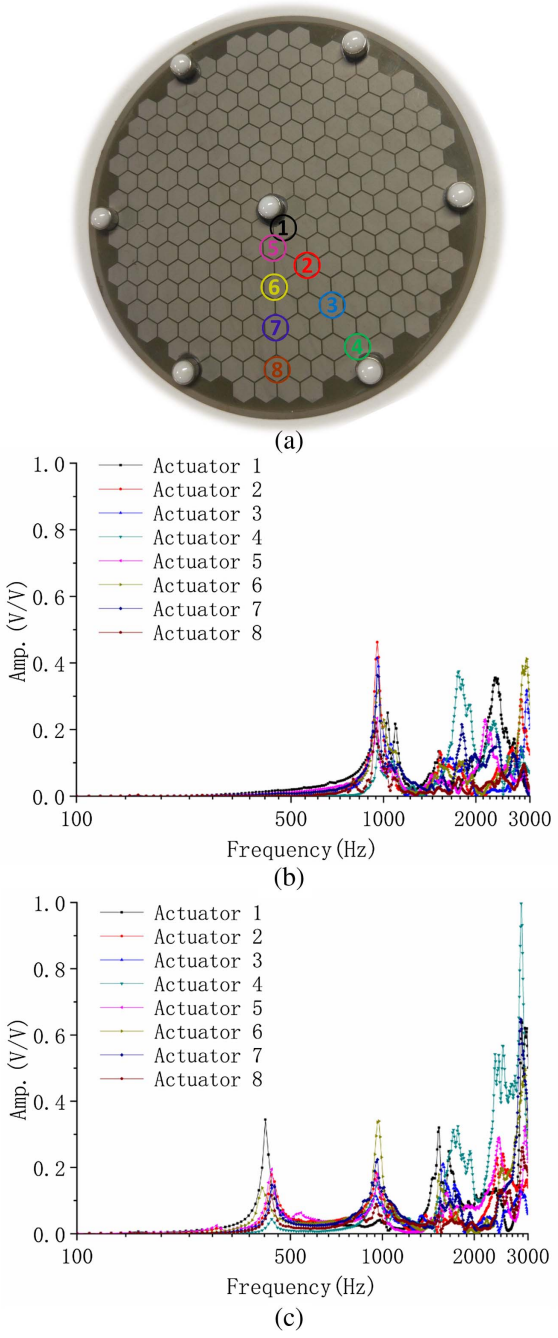

Fig. 6. Amplitude responses of the woofer–tweeter DM when a swept-frequency voltage of 0.5 V was applied on the typical actuators. (a) Positions of typical actuators, (b) responses with all support pillars, (c) response with the center support pillar removed.

correction iterations. Then the residual aberration continues to converge to less than 30 nm wavefront RMS with a PV error less than 0.1 μm. An iterative algorithm based on a steepest-descent algorithm [19] is used in the flattening experiment and the following wavefront reconstruction. For the sake of simplicity, the piezoelectric unimorph and stack are regarded as the same actuators in the controlling algorithm at the price of degrading the convergence efficiency. This is the reason why the wavefront RMS value cannot converge to the level of 30 nm but instead 50 nm within 10 correction iterations. The wavefront profiles after correction show that the reverse deformations mentioned above will be flattened under the cooperation of all the actuators of the DM, especially the actuators near the connecting pillars. The driven voltages in the 100th iteration of correction are depicted in Fig. 7(b).

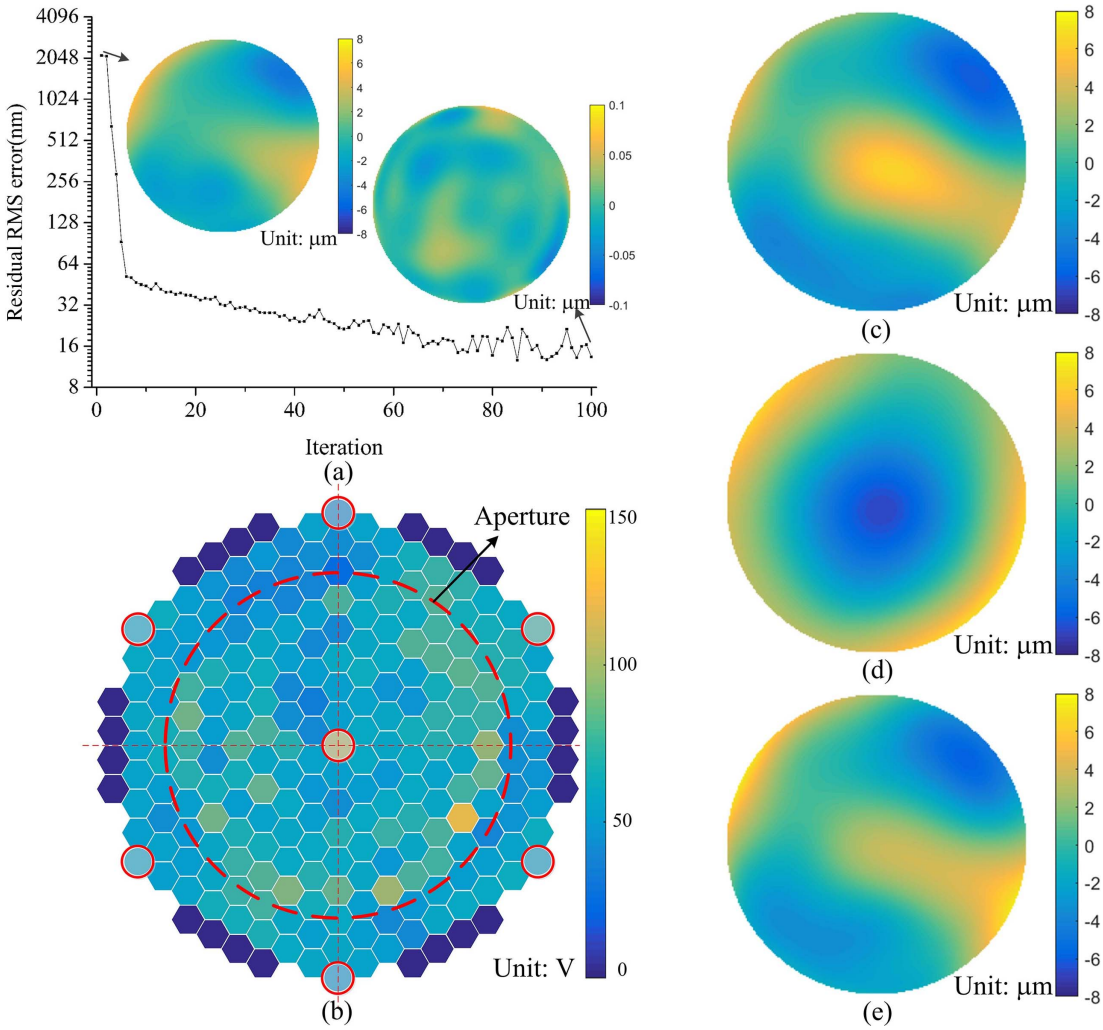

Fig. 7. Results of flattening experiment. (a) Iterative correction evolution with the wavefront profiles before and after correction (tip/tilt was removed) and (b) driven voltage applied on the woofer–tweeter DM. The highlighted driven voltages with solid red circles are applied on the stacks of the actuator array part. (c)–(e) are the simulative wavefronts compensated for by the unimorph part, the simulative wavefront compensated for by the actuator array part, and the simulative wavefront compensated for by both the unimorph and actuator array parts, respectively.

It is noted that the 24 actuators of the outer ring, shown as dark blue pads in the figure, are not used in the flattening experiment and the following experiments. Figure 7(b) shows that the driven voltages of the actuators near the connecting pillars are not obviously larger than the other actuators, which means that the reverse deformations will not significantly affect the correction capabilities of the DM. The wavefront aberrations compensated for by only the unimorph part, by only the actuator array part, and by both the unimorph and actuator array parts can be calculated using the driven voltages shown in Fig. 7(b) and the influence functions measured in this section. The calculated results are shown in Fig. 7(c)–7(e), respectively. The calculated wavefront compensated for by both parts shown in Fig. 7(e) matches the measured initial wavefront aberration before correction shown in Fig. 7(a) quite well with a relative PV difference of less than 15%. There is an inevitable error between the generated aberration and the aberration calculated using the driven voltage and the influence functions because of the nonlinear actuation of the piezoelectric unimorph and stack. In the flattening experiment, the actuator array part mainly generates a large defocus, while the unimorph part generates other aberrations. The unimorph part and the actuator array part work together in the flattening process. It is noted that the deformation distribution shown in Figs. 7(c) and 7(d) is only an alternative solution for flattening. Better algorithms can not only improve the correction efficiency but also optimize the deformation distribution of the unimorph part and the actuator array part. The correction algorithms will be discussed in our further work.

To further evaluate the correction capabilities, the first 35 terms of the Zernike aberrations were reconstructed. In the reconstruction experiments, the DM is actuated to generate Zernike shapes with as large an amplitude as possible while controlling the residual RMS error of the reconstruction to be less than 50 nm. Then, the reconstruction experiment result that has the minimum normalized wavefront error would be chosen to be the best reconstruction result. In the reconstruction experiment, the driving voltages of the unimorph and stack

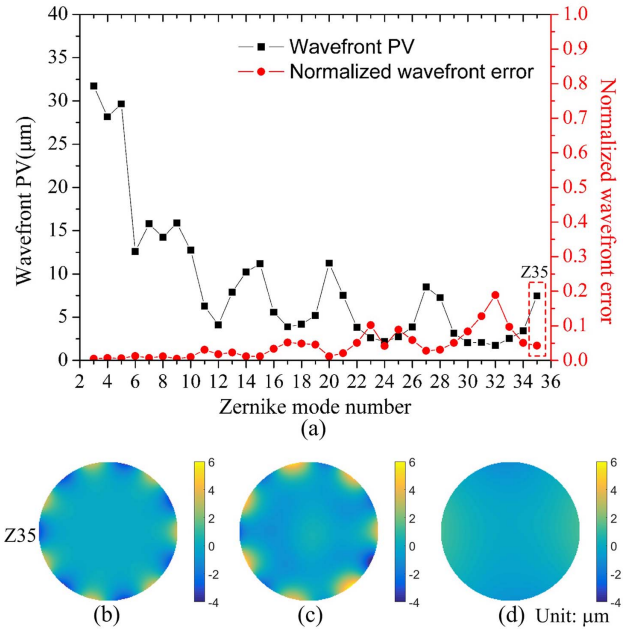

Fig. 8. Reconstruction result of the first 35 terms of the Zernike aberrations. (a) Wavefront PV values and normalized wavefront errors of the reconstructed Zernike profiles, (b) the reconstructed Zernike profiles of Z35, (c) the wavefront profile reconstructed by the unimorph part, and (d) the wavefront profile reconstructed by the actuator array part.

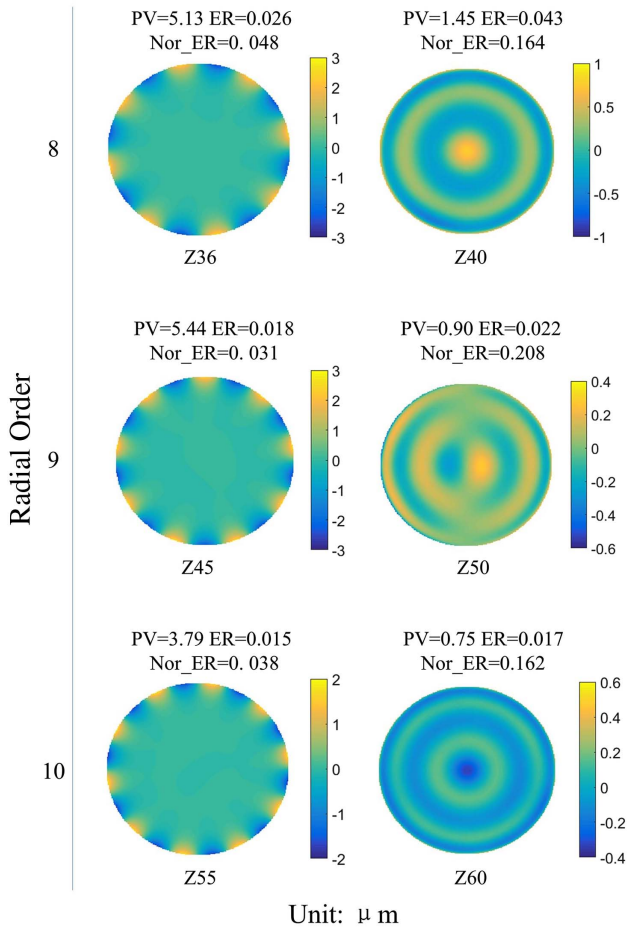

Fig. 9. Reconstruction profiles of some typical Zernike aberrations from the eighth order to tenth order. PV, ER, and Nor_ER are PV values, residual RMS wavefront error, and normalized residual wavefront error, respectively.

actuators were from 0 to 100 V, while the maximum driving voltage is 200 V. The reconstruction results are depicted in Fig. 8. The normalized residual wavefront error is defined as the RMS ratio of the residual wavefront error to the ideal Zernike mode shape, the same as in our previous paper [14]. Hence, the wavefront error in Fig. 8 is the residual RMS of the Zernike shape produced by the DM minus the ideal Zernike shape, normalized to the RMS of the Zernike shape produced. The normalized errors of the first 20 terms are all less than 5% with a PV value more than 3.88 μm. The errors of the first 35 terms are less than 20% with a PV value in excess of 1.73 μm. The normalized errors of reconstruction indicate that the woofer–tweeter DM can generate low-order aberrations with high precision. The PV values of the reconstruction indicate that the woofer–tweeter DM can generate quite large amplitude profiles for low-order aberrations. In conclusion, the woofer–tweeter DM has quite good correction capabilities for low-order aberrations. To illustrate the performance of the unimorph part in higher-order aberration correction, the reconstructed wavefront of 35-term Zernike aberration and the wavefronts generated by the unimorph part and the actuator array part are shown in Fig. 8(b)–8(d), respectively. The PV value of the wavefront generated by the unimorph part is much larger than the PV value generated by the actuator array part. It is indicated that the higher-order aberrations with high spatial frequency are mainly generated by the unimorph part. Some typical Zernike aberrations of a higher order were also reconstructed, as shown in Fig. 9. The normalized residual wavefront error is still less than 20.8% for the 60th term aberration, indicating that the woofer–tweeter DM also has considerable reconstruction capabilities for high-order aberrations up to the 10th order.

5. CONCLUSIONS

To solve the problem of low bandwidth of large-aperture bimorph/unimorph DMs, a woofer–tweeter DM driven by combined actuators with a piezoelectric unimorph and stack is proposed. To optimize the structure parameters, the inherent frequency and deformation of the proposed DM are analyzed. A prototype with a diameter of 100 mm and seven piston actuators was fabricated, and then the correction capabilities of the fabricated DM were experimentally tested. The deformation pattern matches well with the simulations, with the peak value difference and the valley value difference of the measurement and simulative results were less than 0.46 μm and 0.11 μm, respectively. The first resonant frequency of the fabricated DM is about 950 Hz. In the flattening experiment, the aberrations of the fabricated DM were compensated to less than 20 nm. In the reconstruction experiment, the normalized errors of the first 35 terms were less than 20%, indicating the good correction capabilities for low-order aberrations. The simulative

and experimental evaluations indicate that the DM has the characteristics of high spatial frequency and high inherent frequency, which are attractive for astronomical applications. Another advantage of the woofer–tweeter DM is the scalability. A larger woofer–tweeter DM with high bandwidth is under development.

Funding. National Natural Science Foundation of China (NSFC) (51675505); Joint Research Fund for Overseas Chinese, Hong Kong and Macao Young Scientists of the National Natural Science Foundation of China (51628502).

REFERENCES

1. K. Wang and A. Preumont, "Field stabilization control of the European Extremely Large Telescope under wind disturbance," Appl. Opt. **58**, 1174–1184 (2018).
2. E. Stone and M. Bolte, "Development of the Thirty-Meter Telescope project," Curr. Sci., **113**, 628–630 (2017).
3. P. Rausch, S. Verpoort, and U. Wittrock, "Unimorph deformable mirror for space telescopes: environmental testing," Opt. Express **24**, 1528–1542 (2016).
4. Y. M. Guo, A. Zhang, X. L. Fan, C. H. Rao, L. Wei, H. Xian, K. Wei, X. J. Zhang, C. L. Guan, M. Li, L. C. Zhou, K. Jin, J. B. Zhang, J. J. Deng, L. F. Zhou, H. Chen, X. J. Zhang, and Y. D. Zhang, "First on-sky demonstration of the piezoelectric adaptive secondary mirror," Opt. Lett. **41**, 5712–5715 (2016).
5. A. H. Bouchez, D. S. Acton, R. Biasi, R. Conan, B. Espeland, S. Esposito, J. Filgueira, D. Gallieni, B. A. McLeod, E. Pinna, F. Santoro, G. Trancho, and M. A. van Dam, "The Giant Magellan Telescope adaptive optics program," Proc. SPIE **8447**, 84471I (2012).
6. A. Riccardi, M. Xompero, R. Briguglio, F. Q. Pacheco, L. Busoni, L. Fini, A. Puglisi, S. Esposito, C. Arcidiacono, E. Pinna, P. Ranfagni, P. Salinari, G. Brusa, R. Demers, R. Biasi, and D. Gallieni, "The adaptive secondary mirror for the large binocular telescope: optical acceptance test and preliminary on-sky commissioning results," Proc. SPIE **7736**, 77362C (2010).
7. R. Arsenault, R. Biasi, D. Gallieni, A. Riccardi, P. Lazzarini, N. Hubin, E. Fedrigo, R. Donaldson, S. Oberti, S. Stroebel, R. Conzelmann, and M. Duchateau, "A deformable secondary mirror for the VLT," Proc. SPIE **6272**, 62720V (2006).
8. B. Ellerbroek, S. Adkins, D. Andersen, J. Atwood, C. Boyer, P. Byrnes, R. Conan, L. Gilles, G. Herriot, P. Hickson, E. Hileman, D. Joyce, B. Leckie, M. Liang, T. Pfrommer, J.-C. Sinquin, J.-P. Veran, and L. Q. Wang, "Progress toward developing the TMT adaptive optical systems and their components," Proc. SPIE **7015**, 70150R (2008).
9. R. Briguglio, R. Biasi, M. Xompero, A. Riccardi, M. Andrighettoni, D. Pescoller, G. Angerer, D. Gallieni, E. Vernet, J. Kolb, R. Arsenault, and P. Y. Madec, "The deformable secondary mirror of VLT: final electro-mechanical and optical acceptance test results," Proc. SPIE **9148**, 914845 (2014).
10. Y. Minowa, Y. Hayano, S. Oya, M. Watanabe, M. Hattori, O. Guyon, S. Egner, Y. Saito, M. Ito, H. Takami, V. Garrel, S. Colley, T. Golota, and M. Iye, "Performance of Subaru adaptive optics system AO188," Proc. SPIE **7736**, 77363N (2010).
11. R. Arsenault, R. Donaldson, C. Dupuy, E. Fedrigo, N. Hubin, L. Ivanescu, M. Kasper, S. Oberti, J. Paufique, S. Rossi, A. Silber, B. Delabre, J. L. Lizon, and P. Gigan, "MACAO-VLTI adaptive optics systems performance," Proc. SPIE **5490**, 47–59 (2004).
12. R. Donaldson, D. Bonaccini, J. Brynnel, B. Buzzoni, L. M. Close, B. Delabre, C. DuPuy, J. Farinato, E. Fedrigo, N. N. Hubin, E. Marchetti, S. Stroebele, and S. Tordo, "MACAO and its application for the VLT interferometer," Proc. SPIE **4007**, 82–93 (2000).
13. J. Q. Ma, Y. Liu, Y. L. Hu, C. Xu, B. Q. Li, and J. R. Chu, "Low-cost unimorph deformable mirror with high actuator count for astronomical adaptive optics," Opt. Eng. **52**, 016602 (2013).
14. J. J. Chen, J. Q. Ma, Y. X. Mao, Y. Liu, B. Q. Li, and J. R. Chu, "Experimental evaluation of a positive-voltage-driven unimorph deformable mirror for astronomical applications," Opt. Eng. **54**, 117103 (2015).
15. C. Correia and J. Veran, "Woofer-tweeter temporal correction split in atmospheric adaptive optics," Opt. Lett. **37**, 3132–3134 (2012).
16. W. Zou and S. A. Burns, "Testing of Lagrange multiplier damped least-squares control algorithm for woofer-tweeter adaptive optics," Appl. Opt. **51**, 1198–1208 (2012).
17. J. Q. Ma, Y. Liu, T. He, B. Q. Li, and J. R. Chu, "Double drive modes unimorph deformable mirror for low-cost adaptive optics," Appl. Opt. **50**, 5647–5654 (2011).
18. G. Chanan and M. Troy, "Chromatic effects in narrowband phasing of the Keck Telescope segments: theory and numerical simulation," Proc. SPIE **10700**, 107001E (2018).
19. L. J. Zhu, P. C. Sun, D. U. Bartsch, W. R. Freeman, and Y. Fainman, "Wave-front generation of Zernike polynomial modes with a micromachined membrane deformable mirror," Appl. Opt. **38**, 6019–6026 (1999).